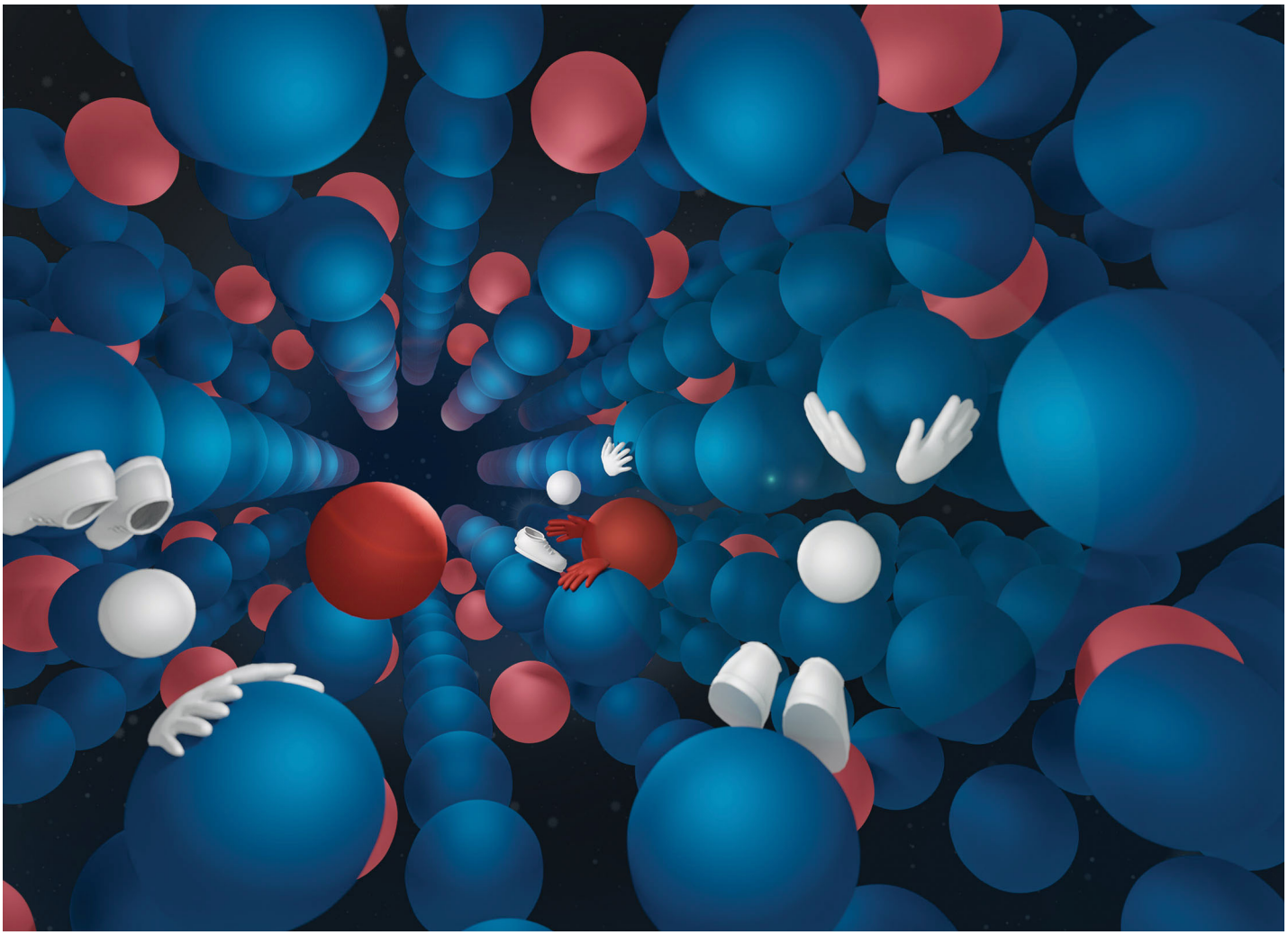

Showcasing research from The Smart Materials Research Institute, Southern Federal University, Rostov-on-Don, Russia. Image designed and illustrated by Mary Bugaeva

In situ formation of surface and bulk oxides in small palladium nanoparticles

In situ synchrotron experiments revealed that the co-presence of hydrogen and oxygen facilitates bulk oxidation in small palladium nanoparticles.

As featured in:

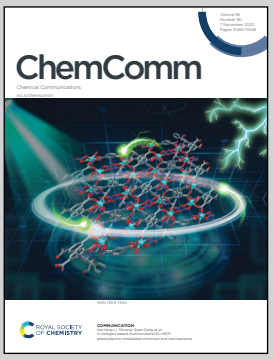

See Aram L. Bugaev *et al.*, *Chem. Commun.*, 2020, **56**, 13097.

ROYAL SOCIETY OF CHEMISTRY

rsc.li/chemcomm

Registered charity number: 207890

ChemComm

COMMUNICATION

View Article Online
View Journal | View Issue

Cite this: *Chem. Commun.*, 2020, **56**, 13097

Received 23rd July 2020,
Accepted 13th September 2020

DOI: 10.1039/d0cc05050d

rsc.li/chemcomm

In situ formation of surface and bulk oxides in small palladium nanoparticles†

Aram L. Bugaev, *[ab] Maxim Zabilskiy, [c] Alina A. Skorynina, [a] Oleg A. Usoltsev, [a] Alexander V. Soldatov [a] and Jeroen A. van Bokhoven [cd]

Evolution of surface and bulk palladium oxides in supported palladium nanoparticles was followed *in situ* using X-ray absorption spectroscopy. The surface oxide was found to be easily reducible in hydrogen at room temperature, while removal of bulk oxide required heating in hydrogen above 100 °C. We also found that the co-presence of hydrogen and oxygen favours a stronger oxidation of palladium particles compared to pure oxygen.

Palladium-based materials have been extensively investigated as catalysts for a wide range of important industrial reactions, such as methane combustion[1–4] and selective oxidation of alcohols.[5–7] Palladium oxide is generally considered to be the actual catalytic species in many of these reactions; however, the activity of metallic palladium or core–shell combinations of Pd and PdO has also been reported.[8–10] A number of previous studies highlighted the importance of the *in situ* detection of palladium oxides and their distribution in the bulk and at the surface of palladium particles to highlight the actual active phase in catalytic oxidation reactions.[5,6]

Oxidation and reduction of palladium phases constitute a very complex process often associated with the formation of core–shell structures.[11,12] Generally, it was shown that the extent of oxidation increases with decreasing particle size and crystallinity of palladium.[8] The surface oxide layer can be formed even at 200 K, while bulk oxidation begins at significantly higher temperatures from 473 K (200 °C). The latter process starts with the formation of an amorphous oxide layer which then slowly transforms into crystalline PdO.[13,14] Such stability of core–shell structures with the surface palladium oxide layer can be attributed to the surface tension of PdO, which is lower than that of metallic Pd.[15] This makes the model with a metallic core and PdO shell energetically more favorable. Formation of such structures was observed also during reduction of the palladium oxide phase. In particular, thermal reduction was associated with a gradual growth of the metallic core inside the PdO particles.[16] However, in the presence of hydrogen the reduction starts with the formation of a metallic Pd surface, which progressively grows towards the bulk.[11] It was reported, that the surface palladium oxide can be fully reduced in hydrogen at 150 °C, while about 50% of the bulk structure remained oxidized, which was explained by the slow diffusivity of oxygen in palladium.[12]

Probing the local atomic and electronic structures around the element of interest using X-ray absorption spectroscopy (XAS) was successfully applied to discriminate the metallic palladium and palladium oxide phases. The extended X-ray absorption fine structure (EXAFS) spectra contain information about the interatomic distances and coordination numbers (CNs)[17] and can directly probe the Pd–Pd and Pd–O coordination in the bulk palladium oxide phases. In addition, X-ray absorption near-edge structure (XANES) spectroscopy probes the unoccupied density of states being therefore sensitive to the changes in the electronic structure due to the chemisorption of the reactive species at the surface of the catalyst and introduction of light impurities (H, C, O) into the palladium lattice, which has a minor effect on EXAFS.[18–21,34]

Here, we combine Pd K-edge EXAFS and XANES analyses to follow the restructuring of the palladium lattice and, respectively, the relative ratio of Pd^{2+}/Pd^{0} in small palladium nanoparticles exploiting the catalytic oxidation of hydrogen as a model reaction. Although XAS is a bulk sensitive technique, the large fraction of atoms at the surface of the nanometer-sized particles provides sufficient sensitivity and enables the detection of both bulk and surface species. In particular, in nanoparticles below 3 nm, more than half of the atoms are located at the surface (where catalytic reaction occurs), which can be successfully monitored by XAS to investigate the

[a] *The Smart Materials Research Institute, Southern Federal University, Sladkova 178/24, Rostov-on-Don, 344090, Russia. E-mail: abugaev@sfedu.ru*
[b] *Southern Scientific Centre, Russian Academy of Sciences, Chekhova 41, Rostov-on-Don 344006, Russia*
[c] *Laboratory for Catalysis and Sustainable Chemistry, Paul Scherrer Institute, Villigen 5232, Switzerland*
[d] *Institute for Chemical and Bioengineering, ETH Zurich, Vladimir-Prelog-Weg 1, Zurich 8093, Switzerland*

† Electronic supplementary information (ESI) available. See DOI: 10.1039/d0cc05050d

catalytic pathways. For this reason, we aimed to achieve a high level of palladium dispersion over a γ-alumina support and to investigate this material *in situ* under hydrogen oxidation reaction conditions.

The prepared Pd/Al_2O_3 catalyst and the γ-alumina support were thoroughly characterized using various physico-chemical methods (Table S1, ESI†). Due to the high BET specific surface area of the utilized γ-alumina support (Fig. S3, ESI†) and the applied gentle thermal treatment during the preparation steps of Pd/Al_2O_3 synthesis, we have achieved a high level of palladium dispersion. Detailed analysis of the XRD patterns of the γ-alumina support and Pd/Al_2O_3 catalyst (Fig. S2, ESI†) revealed the absence of the reflections related to any palladium phase, which can be also attributed to the nanometric dimensions of the palladium particles. Based on the results of H_2 chemisorption (Fig. S4, ESI†), the determined palladium dispersion (*i.e.* the fraction of surface atoms) is 48%. The average particle size estimated using the difference method is 2.3 nm (based on the assumption that palladium nanoparticles exhibit a semi-spherical geometry). STEM analysis (Fig. 1 and Fig. S1, ESI†) revealed the formation of palladium nanoparticles with a mean nanoparticle size of 1.9 ± 0.4 nm.

XAS data show that the initial structure of the catalyst after continuous exposure to air corresponds to that of palladium oxide. The EXAFS fitting using the tetragonal palladium(II) oxide phase (Fig. 2a and Table S2, ESI†) gives an excellent agreement with the experimental data. The cluster size D = (0.5 ± 0.2) nm, determined based on CNs, confirms the formation of small palladium clusters. The lower quantitative value compared to STEM and BET results may be explained by (i) the structural distortion and deviation from an ideal spherical shape and tetragonal crystal structure, (ii) the correlation between D and Debye–Waller parameter (σ^2), and (iii) the fact

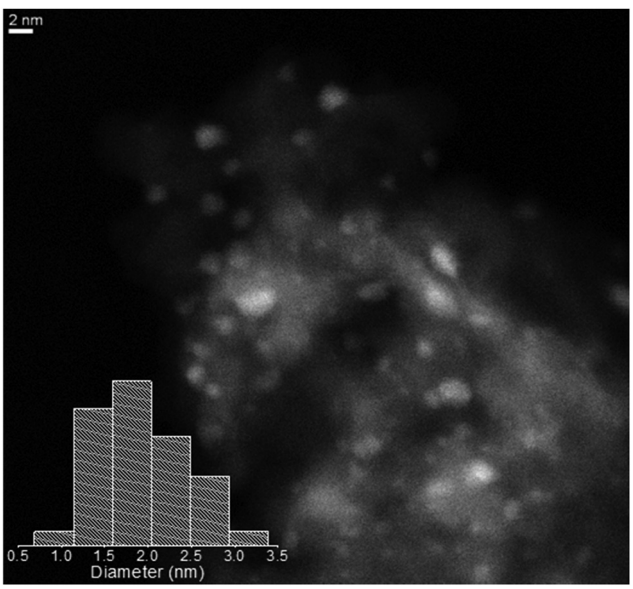

Fig. 1 The HAADF-STEM micrograph of the Pd/Al_2O_3 sample as well as the palladium particle size distribution (inset).

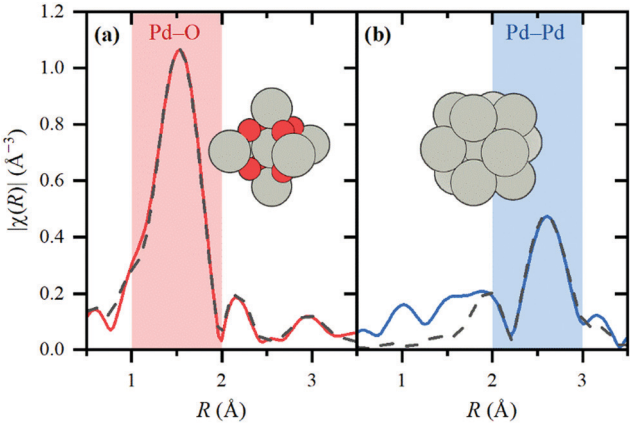

Fig. 2 Experimental FT-EXAFS spectra (solid colored lines) and best fits (dashed grey lines) of the catalyst before (a) and after (b) reduction in hydrogen.

that the smallest particles may escape from STEM detection due to the worse contrast. Notably, the FT-EXAFS signal above 2 Å is almost completely reduced compared to bulk palladium oxide and 2.6 nm PdO nanoparticles (Fig. S7b in ESI†). After exposure to H_2 at 125 °C, the sample was reduced to metallic palladium (Fig. 2b and Table S2, ESI†) with R_{Pd-Pd} = 2.75 ± 0.01 Å. Although significantly reduced in magnitude, all observed peaks in the FT-EXAFS spectra correspond to those in the data for palladium foil and differently sized palladium NPs (Fig. S7a, ESI†),[22,23] indicating the fcc-like structure in the reduced sample. The obtained first shell CN = 6.3 ± 0.9 is lower than CN = 12 of bulk palladium and corresponds to the particle size of *ca.* 1 nm assuming their ideal spherical shape. However, bigger particles with defects and non-spherical shape may also result in similar values for CN.[6] The remaining unfitted background below 2 Å (Fig. 2b) originates from the interaction of surface palladium atoms with the support, the contribution of which to the spectra is considerable due to the small particle size.[23] XANES region before and after reduction is shown in Fig. 3a. No evidence of hydride phase was observed according to the shaping of XANES[18,20,21,24,25] in agreement with the phase diagram for nanometric palladium particles.[21,26–28]

The experimental conditions which were then adopted are summarized in Fig. 3b which also demonstrates the relative fraction of Pd^{2+} and Pd^0 obtained by the linear combination fitting of all experimental data using the spectra before and after reduction, respectively, which are shown in part (a) of the figure. The representative XANES and Fourier-transformed (FT) EXAFS spectra for each region are shown in Fig. 3c and d.

After reduction at 125 °C, the sample was exposed to oxygen (3.3% in He) and immediately cooled down to 50 °C (region 3). A partial oxidation was observed. However, the structure of the nanoparticles did not fully return to the palladium oxide state as in the as-prepared material. The corresponding XANES spectrum (Fig. 3c) is an intermediate between the starting palladium oxide and the reduced phase. The FT-EXAFS signal below 2 Å is enhanced (Fig. 3d) indicative of the Pd–O contribution; however, the dominant peak is the Pd–Pd one at

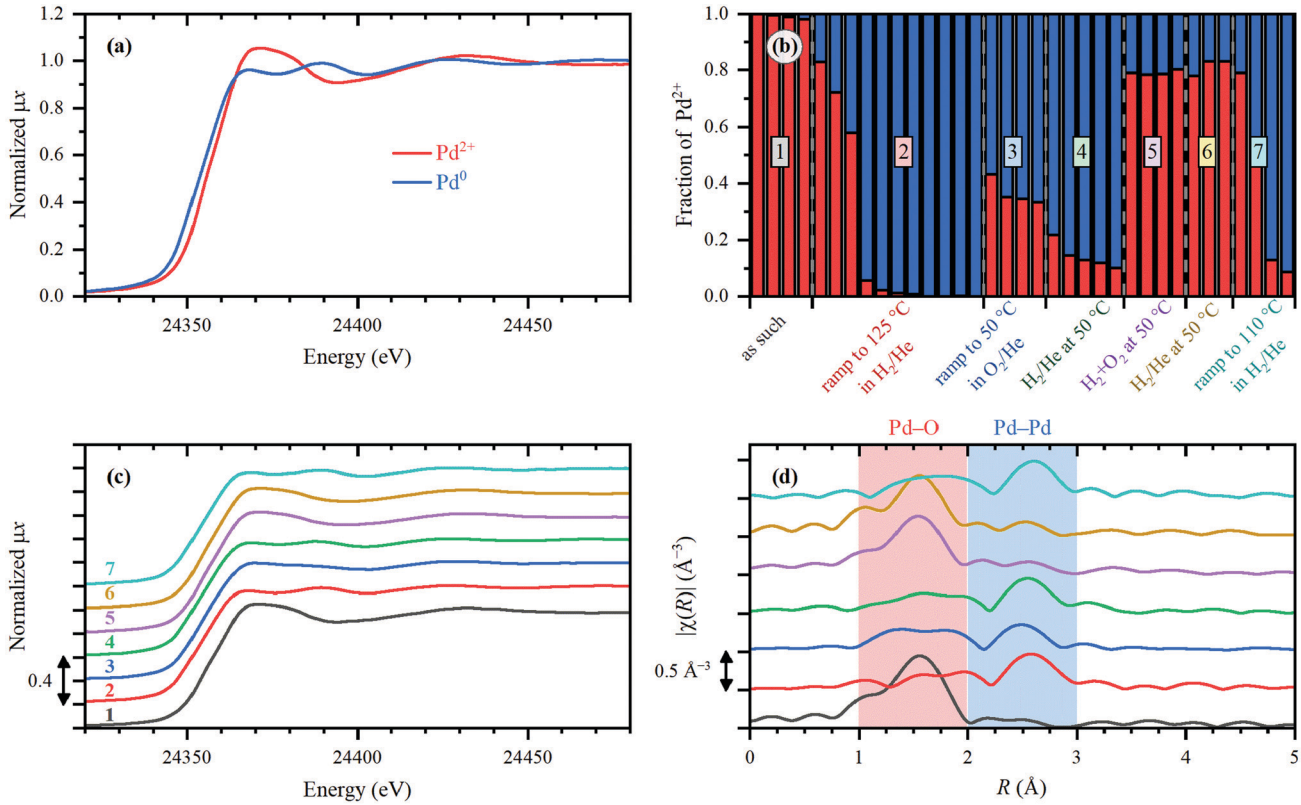

Fig. 3 (a) XANES spectra before (red) and after (blue) reduction. (b) XANES LCA profiles obtained using the two spectra shown in panel (a). Representative XANES spectra and FT of EXAFS from each region of panel (b) are shown in panels (c and d), respectively.

ca. 2.5 Å (phase-uncorrected) as in metallic palladium. Remarkably, these oxidic species gradually disappear already at 50 °C upon reduction in hydrogen (region 4 in Fig. 3b–d).

Then, the sample was cooled to 30 °C and a catalytic mixture of 4.2% H_2/3.3% O_2/He was fed. Under reaction conditions, experimental XANES spectra became identical to the fully oxidized ones with almost complete removal of the Pd–Pd contribution from EXAFS (region 5 in Fig. 3b–d). Interestingly, the formed oxide species were stable in hydrogen at low temperatures (region 6) and were reduced only on heating in hydrogen to above 100 °C (region 7).

A simultaneous view on the evolution of both EXAFS and XANES spectra can provide insights on the surface and bulk distribution of palladium oxides under the reaction conditions. LCA analysis of XANES data allowed us to determine the relative Pd^{2+}/Pd^0 ratio. The principle component analysis (PCA) showed that the dataset is indeed characterized by only two independent components (Fig. S5, ESI†), which is also supported by the isosbestic points in the spectra (Fig. S6, ESI†). This justifies the application of LCA with two components for this dataset. However, the similarity of Pd–O and Pd–OH species in XANES (Fig. S9 and S10, ESI†) may complicate the discrimination of these two species from the experimental data (*i.e.* both will be described by one Pd^{2+} component). Despite the fact that only two different components (Pd^0 and Pd^{2+}) can be discriminated using XANES, different behavior of the species assigned to Pd^{2+} was observed. In particular, the initial structure (1) and the one formed under reaction conditions (5) were reduced only at temperatures above 100 °C, while the one formed upon a small dose of oxygen (3) was reduced at 50 °C. From a general point of view, the easily reducible Pd^{2+} species can be assigned to surface oxides, while the one reduced at higher temperatures is a bulk oxide.

FT-EXAFS spectra support this hypothesis. Indeed, the spectra of the initial structure and the one formed under reaction conditions (spectra 1, 5–6 in Fig. 3) are characterized by a clear Pd–O peak around 1.5 Å (phase-uncorrected) with a much weaker signal of Pd–Pd at 2.5 Å (phase-uncorrected). In spectrum (3), the Pd–Pd signal remains strong as in the spectrum of reduced palladium (2), which means that the overall framework of palladium is similar to the metallic state. At the same time, smooth background below 2 Å (phase-uncorrected) can be explained by surface Pd–O bonds, which are more disordered with respect to bulk oxide to result in a well-defined peak in FT-EXAFS. Thus, under reaction conditions, a stable bulk palladium oxide phase was observed, while in oxygen only surface oxide was formed within the studied time scale (*ca.* 1 h) and oxygen concentration (3.3%).

Formation of a stronger oxide under reaction conditions can be explained by the local heat release due to the exothermic hydrogen oxidation reaction evidenced in Fig. S13 (ESI†). From the other side, palladium is known to adsorb hydrogen forming palladium hydrides with increased Pd–Pd distances.[18,26,29–32] In the presence of hydrogen, the palladium structure becomes

more ''flexible''[33] which may facilitate the restructuring from metallic palladium to its oxide structure. It should be noted that, the range of achieved temperatures (Fig. S13, ESI†) allows the formation of palladium hydrides. However, no significant increase of Pd–Pd distance was observed as can be expected for such small particles.[32] These ultra-small palladium particles also demonstrate much higher stability of the oxide phase compared to bigger particles (*ca.* 3 nm) which were reduced in hydrogen already at room temperature (Fig. S8, ESI†).

To summarize, we have performed the *in situ* XAS study of ultra-small palladium particles under various conditions including catalytic oxidation of hydrogen. Analysis of both XANES and EXAFS spectra allowed discrimination between surface and bulk oxide species. We found that only surface oxide is formed in presence of oxygen at temperatures below 125 °C, which correlates with previous reports for bulk surfaces and supported palladium nanoparticles. The presence of hydrogen facilitates the complete transformation of the metallic palladium particles into bulk palladium oxide already at room temperature. The bulk oxide phase demonstrated stability up to 100 °C in hydrogen, while the surface oxide was readily reduced at lower temperatures. The presence of hydrogen was crucial to form stable bulk oxides at low temperatures due to (i) additional heat realized during hydrogen oxidation and (ii) potential increase of oxygen diffusion in palladium hydride.

The work was financially supported by the Russian Foundation for Basic Research (Grant #19-32-60083 to A. L. B.). The authors acknowledge ESRF for providing the beamtime at Swiss-Norwegian beamline (BM31) for XAS measurements. O. A. U. and A. A. S. acknowledge the President's Grant of Russian Federation for Young Scientists Мк-2554.2019.2 (Agreement No. 075-15-2019-1096) for travel support. We are indebted to Vladimir Dmitriev, Wouter van Beek and Dragos Stoian for their help during the experiment at BM31.

Conflicts of interest

There are no conflicts to declare.

Notes and references

1 D. Ciuparu, M. R. Lyubovsky, E. Altman, L. D. Pfefferle and A. Datye, *Catal. Rev.: Sci. Eng.*, 2002, **44**, 593–649.
2 E. D. Goodman, A. A. Ye, A. Aitbekova, O. Mueller, A. R. Riscoe, T. Nguyen Taylor, A. S. Hoffman, A. Boubnov, K. C. Bustillo, M. Nachtegaal, S. R. Bare and M. Cargnello, *J. Chem. Phys.*, 2019, **151**, 154703.
3 R. J. Farrauto, M. C. Hobson, T. Kennelly and E. M. Waterman, *Appl. Catal., A*, 1992, **81**, 227–237.
4 J. D. Grunwaldt, N. van Vegten and A. Baiker, *Chem. Commun.*, 2007, 4635–4637, DOI: 10.1039/b710222d.
5 J. D. Grunwaldt, M. Caravati and A. Baiker, *J. Phys. Chem. B*, 2006, **110**, 25586–25589.
6 E. Groppo, A. Lazzarini, M. Carosso, A. Bugaev, M. Manzoli, R. Pellegrini, C. Lamberti, D. Banerjee and A. Longo, *ACS Catal.*, 2018, **8**, 6870–6881.
7 H. Yang, S. Li, F. Feng, S. Ou, F. Li, M. Yang, K. Qian, J. Jin and J. Ma, *ACS Sustainable Chem. Eng.*, 2019, **7**, 14621–14628.
8 R. Hicks, *J. Catal.*, 1990, **122**, 295–306.
9 A. Hellman, A. Resta, N. M. Martin, J. Gustafson, A. Trinchero, P. A. Carlsson, O. Balmes, R. Felici, R. van Rijn, J. W. Frenken, J. N. Andersen, E. Lundgren and H. Gronbeck, *J. Phys. Chem. Lett.*, 2012, **3**, 678–682.
10 S. Oh, P. Mitchell and R. Siewert, *J. Catal.*, 1991, **132**, 287–301.
11 S. C. Su, J. N. Carstens and A. T. Bell, *J. Catal.*, 1998, **176**, 125–135.
12 W. E. Moddeman, W. C. Bowling, D. C. Carter and D. R. Grove, *Surf. Interface Anal.*, 1988, **11**, 317–326.
13 X. Guo, A. Hoffman and J. T. Yates, *J. Chem. Phys.*, 1989, **90**, 5787–5792.
14 J. M. Guiot, *J. Appl. Phys.*, 1968, **39**, 3509–3511.
15 S. H. Overbury, P. A. Bertrand and G. A. Somorjai, *Chem. Rev.*, 1975, **75**, 547–560.
16 E. H. Voogt, A. J. M. Mens, O. L. J. Gijzeman and J. W. Geus, *Surf. Sci.*, 1996, **350**, 21–31.
17 J. A. van Bokhoven and C. Lamberti, *X-ray absorption and X-ray emission spectroscopy: theory and applications*, Wiley & Sons, Chichester, 2016.
18 A. L. Bugaev, A. A. Guda, A. Lazzarini, K. A. Lomachenko, E. Groppo, R. Pellegrini, A. Piovano, H. Emerich, A. V. Soldatov, L. A. Bugaev, V. P. Dmitriev, J. A. van Bokhoven and C. Lamberti, *Catal. Today*, 2017, **283**, 119–126.
19 A. L. Bugaev, A. A. Guda, I. A. Pankin, E. Groppo, R. Pellegrini, A. Longo, A. V. Soldatov and C. Lamberti, *Catal. Today*, 2019, **336**, 40–44.
20 A. L. Bugaev, O. A. Usoltsev, A. A. Guda, K. A. Lomachenko, I. A. Pankin, Y. V. Rusalev, H. Emerich, E. Groppo, R. Pellegrini, A. V. Soldatov, J. A. van Bokhoven and C. Lamberti, *J. Phys. Chem. C*, 2018, **122**, 12029–12037.
21 A. L. Bugaev, O. A. Usoltsev, A. Lazzarini, K. A. Lomachenko, A. A. Guda, R. Pellegrini, M. Carosso, J. G. Vitillo, E. Groppo, J. A. van Bokhoven, A. V. Soldatov and C. Lamberti, *Faraday Discuss.*, 2018, **208**, 187–205.
22 M. W. Tew, J. T. Miller and J. A. van Bokhoven, *J. Phys. Chem. C*, 2009, **113**, 15140–15147.
23 V. V. Srabionyan, A. L. Bugaev, V. V. Pryadchenko, L. A. Avakyan, J. A. van Bokhoven and L. A. Bugaev, *J. Phys. Chem. Solids*, 2014, **75**, 470–476.
24 A. L. Bugaev, V. V. Srabionyan, A. V. Soldatov, L. A. Bugaev and J. A. van Bokhoven, *J. Phys.: Conf. Ser.*, 2013, **430**, 012028.
25 A. L. Bugaev, O. A. Usoltsev, A. A. Guda, K. A. Lomachenko, M. Brunelli, E. Groppo, R. Pellegrini, A. V. Soldatov and J. van Bokhoven, *Faraday Discuss.*, 2020, DOI: 10.1039/c9fd00139e.
26 A. L. Bugaev, A. A. Guda, K. A. Lomachenko, V. V. Shapovalov, A. Lazzarini, J. G. Vitillo, L. A. Bugaev, E. Groppo, R. Pellegrini, A. V. Soldatov, J. A. van Bokhoven and C. Lamberti, *J. Phys. Chem. C*, 2017, **121**, 18202–18213.
27 C. Langhammer, V. P. Zhdanov, I. Zoric and B. Kasemo, *Chem. Phys. Lett.*, 2010, **488**, 62–66.
28 C. Wadell, T. Pingel, E. Olsson, I. Zoric, V. P. Zhdanov and C. Langhammer, *Chem. Phys. Lett.*, 2014, **603**, 75–81.
29 A. L. Bugaev, A. A. Guda, K. A. Lomachenko, V. V. Srabionyan, L. A. Bugaev, A. V. Soldatov, C. Lamberti, V. P. Dmitriev and J. A. van Bokhoven, *J. Phys. Chem. C*, 2014, **118**, 10416–10423.
30 T. B. Flanagan and W. A. Oates, *Annu. Rev. Mater. Sci.*, 1991, **21**, 269–304.
31 B. Ingham, M. F. Toney, S. C. Hendy, T. Cox, D. D. Fong, J. A. Eastman, P. H. Fuoss, K. J. Stevens, A. Lassesson and S. Brown, *Phys. Rev. B: Condens. Matter Mater. Phys.*, 2008, **78**, 245408.
32 C. Langhammer, E. M. Larsson, B. Kasemo and I. Zoric, *Nano Lett.*, 2010, **10**, 3529–3538.
33 A. Kawasaki, S. Itoh, K. Shima and T. Yamazaki, *Mater. Sci. Eng., A*, 2012, **551**, 231–235.
34 O. A. Usoltsev, A. Y. Pnevskaya, E. G. Kamyshova, A. A. Tereshchenko, A. A. Skorynina, W. Zhang, T. Yao, A. L. Bugaev and A. V. Soldatov, *Nanomaterials*, 2020, **10**, 1643.

